Table notes: 0

Revision 3

Modeling of trace elemental zoning patterns in accessory minerals with emphasis on the origin of micron scale oscillatory zoning in zircon

Oleg E. Melnik[1*] and Ilya N. Bindeman[2]

[1]Institute of Mechanics, Moscow State University, 119192, 1- Michurinskii prospekt, Moscow Russia

[2]Earth Sciences, 1272 University of Oregon, Eugene OR 97403

*corresponding author melnik@imec.msu.ru

Abstract. We present a numerical model of trace element oscillatory zoning patterns formed when zircon crystallizes from silicate melt which is also appropriate for other accessory phases with known partition and diffusion coefficients and saturation conditions. The model accounts for diffusion-controlled accessory mineral growth and the equilibrium crystallization of major mineral phases. Consideration of recent, experimentally-determined dependencies of partition coefficients on temperature, we find that thermal changes provide the simplest explanations of oscillatory zoning in accessory minerals. Numerical experiments with different cooling rates explore different crystallization scenarios with and without the precipitation of other phases and/or the interface reaction of phosphorus (P) and yttrium (Y) to form xenotime. However, these processes are monotonically related to growth rate and do not cause oscillations. Minor 3-10°C variations in temperature do not result in zircon dissolution, but strongly influence

zircon growth and lead to variations in coeval Y, Hf, and rare earth element (REE) concentrations of up to a factor of two, comparable to those observed in nature. Such temperature variations may be very common in any igneous body in response to external factors such as replenishment by hotter magmas or convection. More significant temperature fluctuations may result in initial minor dissolution at higher temperatures during a mafic recharge event but with continuous growth afterwards. At high temperature (>~850°C) the amplitude of oscillations is relatively small that confirms observations of both less common oscillatory zoning in hot and dry volcanic rhyolites and abundant oscillations in plutonic zircons and in zircons in cold and wet crystal-rich mushes. Additional oscillations in zircon are modeled in response to oscillations of pressure on the order of ±35-50 bars, causing water concentration fluctuations of ±0.1 wt% in water-saturated melt cells with a gas bubble. These variations cause variations of Zr diffusion and zircon growth rates. Such fluctuations could result from pressure oscillations due to recharge and convection in the magma chamber. All simulated runs generate smoothed oscillatory growth zoning; similar patterns found in nature may not necessarily require post-growth intracrystalline diffusion.

Keywords: Accessory minerals, numerical model, diffusion equation, crystal growth, oscillatory zoning

1. Introduction

1.1. Oscillatory zoning in minerals

Oscillatory zoning (**Fig. 1**) in igneous minerals is a phenomenon that has fascinated microscopists for more than 150 years (Bunsen, 1851, Bowen, 1928; Corfu et al. 2003). It is typically defined as micron to submicron-scale chemical oscillation and is observed in nearly all accessory minerals of constant composition, and in major minerals (plagioclases, pyroxenes), which are commonly solid solutions. Oscillatory zoning occurs in terrestrial and extraterrestrial (e.g. lunar, meteoritic) objects, in minerals crystallizing from both magmas and hydrothermal solutions. Chemical oscillations affect both major, minor, and trace elements with amplitudes of variation from 10s of percent to a factor of 2 to 3. We here distinguish three types of oscillatory zoning that can have different explanations: i) oscillations of major elements in a mineral solid-solution (e.g. plagioclase, pyroxene); ii) oscillations of a minor or trace element in a major phase (e.g. Ti, Al in quartz); and iii) oscillations of trace elements in an accessory phase (e.g. REE in zircon and monazite).

Earlier work on oscillatory zoning of major elements in major phases such as plagioclase (Vance, 1962; Wiebe, 1968; Sibley et al. 1976) has resulted in several explanations that invoke both internal and external factors. For major solid solutions (plagioclase, pyroxenes), the partitioning of major components is determined by changes in temperature along liquid lines of descent. However, the solid/melt partition coefficients of major oxides (for example CaO or Al_2O_3 in an albite-anorthite-diopside system (Morse, 1994) or in crystallization modeling in MELTS; Ghiorso and Sack, 1995) are ≈1 and do not change by more than one order of magnitude between the liquidus and solidus temperatures. The constituent major elements in these minerals have comparable and often

coupled (Liang et al. 1994) diffusion coefficients in melts surrounding crystals for all elements, except for ~10 times faster-diffusing alkalis (Zhang et al. 2010).

For major minerals with near-constant composition (e.g. Quartz), partition coefficients of oscillating components such as Ti, Al, K, and other recently explored elements are very small ($<10^{-2}$), while their diffusion coefficients are larger than Si (Zhang et al. 2010). An additional feature of these minerals is that the partition coefficient has a very steep and strong dependence on *T,* which is utilized in several single-element thermometers (Wark and Watson, 2007; Hayden and Watson, 2007; Thomas et al. 2010*)*. These elements occur in the melt in 0.1 to a few wt% levels, and are subject to activity-composition relations affecting the partition coefficient (*K*) via Henry's Law constants that vary with the activities of other components, a subject of much recent discussion for Ti-in-quartz incorporation (Thomas et al. 2010).

This paper is about the zoning of trace elements in accessory minerals (zircon, apatite, rutile and others), minerals commonly of largely constant composition that are very important for geochronology and the trace element evolution of their host magmas. Much work has been performed on zoning in zircon (**Fig. 1**) as revealed by cathodoluminescence imaging (Marshall, 1988). For such accessory phases *K* and saturation are strong functions of *T* and depend little on activity-composition relations and on phase diagrams (e.g. Watson and Harrison, 1983), and the following observations/distinctions can be made: 1) the mineral-forming elements for these minerals are commonly trace elements themselves and they do not control the phase relations in the bigger system (e.g. Neogi et al. 2014). 2) The behavior and crystallization of these accessory minerals is simply explained by saturation at a certain temperature and

continuing crystallization with decreasing temperature (Watson and Harrison, 1983; Rubatto and Hermann, 2007; Hayden and Watson, 2007). Saturation concentrations are typically very low (hundreds of ppm), leading to very high *K* values of mineral forming trace elements: 490,000 ppm of Zr in zircon/hundreds of ppm in melt leads to $K = \sim 10^3\text{-}10^4$ for zircon, for example. 3) The diffusion coefficients of their constituting 3+ to 5+ elements are typically slower than for silica and other major oxides (e.g. Zhang and Ni, 2010). 4) Unlike major phases, the growth rates for most accessory phases are slow and are rate-controlled by slow diffusion of a single minor or trace element of low concentration in the melt: Zr for zircon, P for apatite, REE or P for monazite, Ti for rutile and titanite, REE for chevkinite, etc. These relationships explain why accessory minerals are small and scattered with large spatial separation between major minerals; such relationships justify the use of a simple 1D diffusion-growth model in spherical coordinates with two moving boundary conditions that we employ here (**Fig. 2**). The rest of discussion will be centered on zircon (**Fig. 1**), but the conclusions should be applicable to other accessory phases.

1.2. Trace element partitioning in zircon, element coupling, and co-crystallization of other phases

Trace elements entering zircon obey Onuma-type partitioning relationships (e.g. Hanchar et al. 2001; Hanchar and van Westrenen, 2007) with elements of the same valence group and with sizes closest to those of the sites of preferred substitution (e.g. Hf) having far greater partition coefficients than smaller or larger ions (e.g. Ti). The variations in trace element concentrations do not change the Henry's Law constant, *K*, although for

elements with a concentration of just a few ppm, such as Ti in zircon, defect site partitioning has been proposed (Fu et al. 2008).

REE, Y, Sc other 3+ elements, and also 5+ elements require charge compensation when diffusing in the 4+ crystal structure of zircon. Entry of both REE and 5+ elements into zircon is commonly explained by xenotime-type substitution, $P^{5+}+Y^{3+} = Si^{4+}+Zr^{4+}$, that should lead to a 1:1 covariant line of P and Y concentrations (Hanchar et al. 2001). Reviewing the literature and from our own considerations below, we cannot say with certainty that trace element coupling is the controlling phenomenon in trace element partitioning, due to the exceedingly low abundances of trace elements. Furthermore, many studies of natural samples have demonstrated both molar excess and deficiencies of P with respect to SUM ($REE^{3+} + Y^{3+}$) suggesting that xenotime-type substitution is not the only possibility for Y and P entrance into zircon (Finch et al. 2001). DeHoog et al. (2014) suggested that H^+ plays an important role in charge compensation and promotes the partitioning of trace elements into zircon and Trail et al. (2016) considered the role of Li. An alternative explanation is the independent entry of trace elements generates vacancies into zircon in accordance to the Henry's Law constants of each element.

A way to empirically test for coupling, or a lack thereof, in element partitioning is to consider elemental covariations in oscillatory zoned zircons (**Fig. 1**). For illustrative purposes in this study we performed measurements of trace elemental variations in zircons from silicic systems spanning from cold, near solidus conditions to hot, near liquidus conditions, the Fish Canyon Tuff, Young Toba tuff, and major Yellowstone tuffs, respectively (**Fig. A1**). Our measurements agree with previous data and are suggestive of covariation between elements, but without a 1:1 relationship. These considerations also

have implications for the origin of elemental zoning patterns, and in particular on whether such coupling leads to oscillations. An additional important factor in generating trace elemental variations in zircons is the co-crystallization of additional phases that happen to partitions the very same elements. This process commonly occurs in nature (e.g. zircon co-crystallizing with sphene and apatite). For example, if crystallization of apatite happens together with zircon, the residual melt as well as zircon may become depletedin P. However, the rate of "signal" transfer from apatite to zircon (i.e. P concentration in the melt) will be dependent on the diffusion coefficient of P and the mean distance between zircon and apatite crystals. Crystallization of both accessory phases is controlled by simple saturation conditions rather than by complex reactions, and so saturation and rates of diffusion are controlled by temperature, which in turn controls trace element/melt partitioning coefficients.

We thus search for the simplest physical explanation of oscillatory zoning phenomena by considering temperature and water content fluctuations and their effect on experimentally–determined saturation conditions, and diffusion, and partition coefficients. We explore if this simplest model is sufficient to explain patterns of trace element distribution in zircon, including 1) the length scale, amplitude, and relative position of the modeled elements, 2) the magnitude of temperature changes that are required to explain naturally observed mineral zoning, and 3) the influence of the co-crystallizing major phases. Then we devote attention to the effect of coupled substitutions and show that if present, these does not lead to compositional oscillations.

2. Model

2.1 Mathematical model

The present model is provided as a in MATLAB code in spherical coordinates with two moving boundary conditions (**Fig. 2**), which represents a development of the model of Bindeman and Melnik (2016) of zircon growth/dissolution within a cell of melt with another phase(s) on the outer boundary whose composition is controlled by a phase diagram. In the earlier model we emphasized elemental concentrations/profiles in the melt cell surrounding the zircon; in the present paper we compute elemental concentrations within zircon and monitor their changes in accordance with partition relations and other factors explained below. The model setup is shown on **Fig. 2** and includes a spherical zircon in its center. The model numerically reproduces the enrichment/depletion of compatible/incompatible elements during the diffusion of ions toward the growing zircon crystal in the center of the cell. Likewise, the crystallization of other (major and trace) minerals around the zircon on the outer melt cell boundary may enrich or deplete the melt in trace elements. These are implemented by a choice of boundary phase identities and proportions, which determines the bulk partition coefficients of the elements of interest between the melt and the outer boundary. The temperature within the melt cell surrounding the zircon is uniformly changing and is assumed to be a function of time because the thermal diffusivity is several orders of magnitude higher than the chemical diffusivity within a cell, so temperature equilibrates instantaneously on the timescales of zircon growth.

The transport of Zr and trace elements in the melt cell is governed by the standard diffusion equations that in a spherical case can be written as:

$$\frac{\partial C_i}{\partial t} = \frac{D_i(T)}{r^2}\left(\frac{\partial}{\partial r} r^2 \frac{\partial C_i}{\partial r}\right);\ i = Zr, tr \qquad (1)$$

Here C_i is the concentration of i-th element, measured in ppm, r is the radius counted from the center of the zircon crystal, and t is the time. Eq. (1) is solved only inside the melt part of the cell, $s < r < R$, because the diffusion of Zr and trace elements in the crystal phase is very slow in comparison with diffusion in the melt.

Boundary conditions at the crystal-melt interface ($r = s$) ensure local thermodynamic equilibrium, mass conservation of Zr and trace elements, and the partition of trace elements.

$$r = s : -D_i \left.\frac{\partial C_i}{\partial r}\right|_{r=s} = J_i = V\left[C_i^m - C_i^s\right];\ C_{Zr}^m = C_{sat}\left(T\right), C_{Tr}^s = K\left(T\right)C_{Tr}^m. \qquad (2)$$

Here V is the linear growth rate of zircon, C_i^m is the concentration of Zr and trace elements in the melt attached to the growing zircon crystal, C_{Tr}^s is the trace element concentration in zircon, and C_{Zr}^s = 490,000 ppm is Zr concentration in zircon. The saturation concentration C_{sat} of Zr mainly depends on temperature and melt composition which are governed by equations in Watson and Harrison (1983) and Boehnke et al. (2013) and integrated into the model. In the simulations presented below we use Boehnke et al. (2013) formulation with the value of M-factor equal to 1.62 appropriate for low silica "monotonous intermediate" felsic magmas that exhibit oscillatory zoning. $K(T)$ values are the partition coefficients of trace elements of interest between the melt and the zircon crystal.

On the outer melt boundary ($r = R$), mass partitioning of Zr and trace elements between major minerals and the melt is specified:

$$r = R : -D_i \left.\frac{\partial C_i}{\partial r}\right|_{r=R} = J_i = W\left[C_{m,i} - C_{X,i}\right];\ C_{X,i} = kC_{m,i}. \qquad (3)$$

Here W is the velocity of the outer boundary controlled by changes in the melt fraction due to crystallization of major minerals, C_X is the concentration of zirconium and trace elements in major minerals, and k is the distribution coefficient $C_{Zr}^{major}/C_{Zr}^{melt}$. In order to determine W we use phase diagram (solidus-liquidus) relations for a typical granitic melt after the crystallization experiments of Piwinskii (1968, composition 102 at 2 kb):

$$x = 3.1\Theta - 8.9\Theta^2 + 12.3\Theta^3 - 5.46\Theta^4,$$
$$\Theta = \frac{T - T_S}{T_L - T_S},\ T_S = 973\,K, T_L = 1203\,K. \qquad (4)$$

Here x is the melt fraction and Θ is the dimensionless temperature. A discussion of the effect of changing the parameters in eq. (1-3) will be presented below.

The current model that monitors trace element concentrations and behavior within zircon does not allow for the modeling of zircon dissolution, because it does not store the trace element distribution within zircon. Thus, it cannot calculate mass balances for trace elements (eq. 2) correctly for negative values of the velocity, V, as linear partitioning between the melt and the crystal does not work during dissolution. However, the present model as is shown below is able to simulate zircon oscillatory zoning with slow growth rather than by zircon dissolution.

2.2. Properties of species: diffusion and partitioning relations

As zirconium diffusion in melt is strongly dependent on temperature and water content (Watson and Harrison, 1983), we use the parametrization from Bindeman and Melnik (2016) for the Zr diffusion coefficient D_{Zr} and the equilibrium melt saturation $C_{sat}(T)$ as:

$$\ln(D_{Zr}) = -\frac{11.4X_{H20}+3.13}{0.84X_{H20}+1} - \frac{21.4X_{H20}+47}{1.06X_{H20}+1} \bullet \frac{1000}{T} \quad \text{(5a)}$$

$$C_{sat} = 490000 / \exp\left(\frac{10108}{T} + 1.16(M-1) - 1.48\right) \quad \text{(5b)}$$

As this work considers not only zircon growth but also the incorporation of other elements in zircon, diffusion coefficients for Zr and other trace elements in the melt are taken from a compilation by Zhang et al. (2010). **Figure 3a** shows the values of trace element diffusion coefficients normalized to Zr diffusion coefficient at X_{H20}=3 wt.%. We assume that Dy^{3+} and Y^{3+} diffusion coefficients are equal. Ti^{4+} is the fastest diffusing element followed by Zr^{4+}, then Y^{3+}, Dy^{3+}, other REE^{3+}, and Hf^{4+} are within one log unit from Zr^{4+}, and finally P^{5+}, U^{4+} and Th^{4+} are significantly slower. This order is in line with the faster diffusion of smaller, lesser charged elements in silicate melts (e.g. Hahn et al. 2005).

Partition coefficients of the trace elements between zircon and silicic melt are presented in **Fig. 3b** and range from ~ 4 for P to more than 3000 for Hf (Rubatto and Hermann, 2007). The Rubatto and Hermann (2007) experiments were conducted at lower temperatures (800-1000°C) than many previous ones dealing with zircon saturation (e.g. Harrison and Watson, 1984), and extrapolation of partition and saturation data to the lowest (650-750°C) *T* is still required. We note the steep dependence of partition coefficients on temperature for most elements with the steepest dependence being for Y, as has been noted before in many other experiments involving accessory phases (e.g monazite, apatite, garnet, Zhang et al., 2010).

Coupled substitution of major and trace elements of different valence groups (e.g. $P^{5+} + Y^{3+} = Si^{4+}+Zr^{4+}$) in zircon is much discussed topic, with natural and experimental

evidence both supporting and contradicting it (Hanchar et al 2004; Hoskin and Schaltegger, 2009; Trail et al; 2016 and references therein). To see if coupled substitution matters for oscillations, we defined the boundary conditions to allow and disallow coupled substitution at the growing zircon surface. With respect to diffusion in the silicate melt, different trace elements diffuse independently as there are several charge compensating mechanisms in the melt involving major elements (e.g., Zhang et al., 2010). Elemental groups or cluster formation in the vicinity a zircon-melt interface where 3+ and 5+ and 1+ elements compete is of much interest (Rustad, 2015), but has not been determined with certainty. In the present numerical model, we treat each element independently with respect to its experimentally-determined diffusion and partition relations as is shown in **Fig. 3**. Expressions for trace element diffusion and partition coefficients can be found in supplementary MATLAB code (functions TraceDiff and Kdd, respectively). In section 3.2 we explore the effect of coupled P and Y incorporation into the zircon.

Diffusion of 3+, 4+ and 5+ trace elements in zircon is too slow (Cherniak et al. 1997a, b) to affect their distribution on volcanic and even plutonic timescales, and in the modeling below we ignore trace elemental redistribution in zircon upon capture. Some diffusional relaxation of the originally step-function or sawtooth profile in zircon is possible on submicron scales, especially in hotter and longer-lived systems given these published diffusion coefficients, but this will not affect the observed zonation on larger scales.

2.3 Numerical algorithm

The model was written in MATLAB and used an unconditionally stable implicit formulation for the discretized diffusion equation in a fixed frame domain by using a tri-

diagonal matrix (Thomas method) algorithm. Details of the numerical method are presented in Bindeman and Melnik (2016) for pure zircon growth. We solve Eq. (1) with boundary conditions (2,3) independently for each trace element. Zircon growth rates are obtained from the solution of the diffusion equation for zirconium. Changes in the melt fraction and the corresponding velocity of the outer cell boundary are governed by temperature changes only along specified phase diagram given by Eq. (4).

3. Results

3.1 Zircon crystallization from melt and partitioning relations during monotonic cooling

We first consider a scenario of zircon crystallization from a melt cooling at a constant rate in order to detect any oscillatory zoning of trace elements naturally resulting from crystallization histories of their host magmas in the framework of our model. **Figure 4** shows calculated profiles in the melt for normalized concentrations of Zr (dashed line) and trace elements at the final temperature for the simulation of zircon growth during a linear temperature drop from 840 to 720°C over 5000 years from a 2 mm melt cell with no major mineral crystallization (W=0, **Fig. 2**). As the temperature decreases the zircon starts to grow and a diffusive boundary layer with a decreased concentration of Zr and other strongly compatible elements (the "trough") is formed and persists for the entire duration of crystallization in all models.

The zircon growth rate is determined by the diffusion of zirconium towards the crystal-melt interface (e.g. Harrison and Watson, 1984). Both the diffusion and partition coefficients play a role in the formation of boundary layers in trace element

concentrations. The boundary layer is strongly depleted in Hf because its partition coefficient is large and its diffusion is slower than that for Zr. U diffuses faster than Th, but has much higher partition coefficient resulting in stronger depletion in the boundary layer. Dysprosium and Y diffuse at the same speed in our model, but Y is more compatible than Dy, thus the boundary layer is more strongly depleted in Y. P, which has a small diffusion coefficient similar to U, is only slightly compatible in zircon and remains relatively concentrated in the melt phase adjacent to the zircon despite its slow diffusion. If the temperature stops decreasing at T = 800°C in our model, the depletion disappears in ~5 ka, making it possible to detect last stage of zircon growth if it is quenched later due to a rapid T drop or H_2O loss (which affects diffusion coefficients of Zr dramatically, as Bindeman and Melnik (2016) documented in glasses adjacent to zircon the Summit Lake flow of Yellowstone; **Fig. 18**).

Because all modeled trace elements (excluding P and Ti) have K>>1 in zircon, no piling up effects are possible for zircon and other accessory minerals with similar partitioning near the boundary. Indeed, the opposite may be true resulting in boundary layer depletion. This simple consideration of high K and slow diffusion eliminates one possible mechanism of oscillatory zoning in accessory phases, that is otherwise suggested for plagioclase, for example, (e.g.,Sibley et al. 1976). However, bulldozing effects can be present on the outer melt boundary and lead to a piling up of trace elements as a function of W and k. (**Fig. 2** also see Bindeman and Melnik, 2016). Oscillatory temperature changes cause crystallization of the major minerals on the outer boundary (**Fig. 2**), causing the propagation of compositional diffusion waves towards the growing zircon in the center. However, these compositional waves are modulated by the relatively long distance

in melt cell around the zircon, and the slow elemental diffusion on short timescales. Thus, major element growth oscillations due to crystallization of a major mineral are dampened, and compositional "waves" from major element growth oscillations are not reflected in zircon zoning.

Figure 5 shows the distribution of trace elements within the zircon crystal as a function of its radius. High diffusivity and a sharp increase in the partition coefficient of Y with a decrease in temperature result in the enrichment of the zircon crystal in Y as crystallization proceeds. The large partition coefficient and relatively slow diffusivity of Hf result in the depletion of the boundary layer in Hf and a consequent decrease in the Hf concentration in the growing zircon. There are also smaller increases in U, Th, and P towards the zircon rim due to an increase in partition coefficient at low temperatures (**Fig. 3b**).

Another important trace element that enters the zircon structure is Ti, which is used in many other geochemical and geothermometry studies (e.g. Ferry and Watson, 2007). We plot for reference the variation of Ti content in zircon using Eq. (15) from Ferry and Watson 2007 with activities of SiO_2 and TiO_2 equal to 1 and 0.65, respectively, as is accepted by the above authors. There is a progressive decrease in Ti concentration within zircon during crystallization and at lower temperatures as Ti is a fast diffuser compared to Zr and zircon growth does not produce elevated concentrations at the boundary layer, despite Ti's small partition coefficient.

It is important to note that our numerical modeling assuming monotonic temperature decreases from high to low T along a linear path produces no sign of oscillatory zoning. This result holds in a wide field of parameter space and is independent

of the cooling rate (ranging from 10° to 0.01°C/yr). Further experimentation with non-linear but smooth temperature paths, characteristic of cooling intrusions, ranging from concave-down exponential to concave-up square root also show no sign of oscillatory zoning. This is simply explained by the absence of a feedback between boundary layer concentrations of trace elements and the zircon growth rate, which is controlled solely by the diffusive flux of Zr. Zircon itself grows monotonically with respect to cooling in our numerical experiments (this work and Bindeman and Melnik, 2016).

The numerical simulations presented above show large (up to 0.4 wt%), concentrations of P (**Fig. 5**) in zircon at the later stages of the growth due to larger values of the partition coefficient of P at low temperatures (see **Fig. 3b**). The increase in P content is comparable to Y, in agreement with data where both elements are measured (e.g., Aranovich et al. 2016), although Y and P commonly show a variety of zoning patterns (Hoskin and Schaltegger, 2009; Hanchar et al. 2001a,b ; Hoffman et al. 2009; Trail et al. 2016). There are several possible explanations for this. First, partition coefficients of P in zircons and their *T* dependence are poorly known, and, second, the simultaneous growth of apatite, which always co-precipitates with zircon, will reduce the phosphorus content in the melt to the apatite saturation level, and consequently the P concentration in zircon will drop down.

3.2 Interface kinetic reactions

The incorporation of P and Y into zircon may not be completely independent from one another, as is proposed in many studies (Hoskin and Schaltegger, 2009 and references therein) under the xenotime-type substitution mechanism $Y^{3+}+P^{5+} = Si^{4+}+Zr^{4+}$. If so, the

very high partition coefficients predicted by extrapolation of high-T to low-T data (**Fig. 3**) may be mitigated by the interface-xenotime formation reaction that we now consider. If the interface exchange reaction plays an important role for the entry of heterovalent elements into zircons, then other charge compensating mechanisms described in the introduction may also lead to the outcome that elements influence each other's partitioning relations. Here, we model xenotime substitution into zircon, which is explained by its formation reaction:

$$Y^m + P^m = X^s \tag{6}$$

We assume that xenotime does not independently nucleate in the melt because Y concentration is low, but rather forms only at the zircon's surface during incorporation into the crystal where the concentrations of Y is the highest due to the very high partition coefficient (**Fig. 3b**), and thus reaction (6) is shifted to the right at the surface of zircon, where xenotime likely forms in nanoclusters. The formation and destruction of the xenotime can be modeled with forward and reverse reaction constants of the first order reaction, k_f and k_r.

To check if P and Y coupled substitution can cause oscillatory zoning of the xenotime component in zircon we use the results from a linear temperature drop run and solve diffusion equations for P and Y with modified boundary conditions:

$$\begin{aligned}
-D_i \left.\frac{\partial P}{\partial r}\right|_{r=s} &= V\left[P^m - P^s\right] - \frac{\left(k_f PY - k_r X\right)}{2};\ P^s = K_P\left(T\right)P^m, \\
-D_i \left.\frac{\partial Y}{\partial r}\right|_{r=s} &= V\left[Y^m - Y^s\right] - \frac{\left(k_f PY - k_r X\right)}{2};\ Y^s = K_Y\left(T\right)Y^m, \\
\left.\frac{\partial X^s}{\partial t}\right|_{r=s} &= k_f PY - k_r X - VX^s,\ X^s = K_x\left(T\right)X^m.
\end{aligned} \tag{7}$$

Here P, Y and X are the concentrations of phosphorus, yttrium and xenotime, respectively, and k_f and k_r are the reaction rates for the forward and reverse reactions of xenotime formation and dissociation. We assume that xenotime is unstable (not saturated) far from the zircon-melt interface and, thus, we do not solve the diffusion equation for X in the melt. Yttrium and P diffuse independently to the boundary and xenotime is only formed in the very narrow surface boundary layer adjacent to zircon. For this simulation, we can assume that only xenotime can be incorporated into the zircon structure. In this case the partition coefficients of P and Y, K_P and K_Y, are equal to zero. As an initial condition we assume an equilibrium xenotime concentration: $X(t=0)=k_f P(0)Y(0)/k_r$.

Figure 6 shows the xenotime distribution within the zircon for different values of K_X for $K_P = K_Y = 0$. Due to the decrease in Y concentration in the melt, the formation of xenotime progressively slows down resulting in lower concentrations of X in the zircon as the crystal grows. The decrease in concentrations of both P and Y occurs monotonically but we do not observe oscillations with respect to either element. Thus, the coupled substitution of P and Y cannot be a cause of oscillatory zoning in zircon as the interface exchange reaction is *linearly* proportional to the concentrations of the elements or their products as is explained in Eq. (6). However, this mechanism of coupled substitution may help mutual partitioning of P and Y, especially when there is a 1:1 molar relationship as is observed in some studies (Hoskin and Schaltegger, 2003).

3.3. Temperature oscillation effects on growth rates and Zr concentrations

Next, we investigate how small temperature variations can result in non-monotonic changes in crystal composition and zircon zoning patterns. A series of simulations with a sinusoidal temperature drop (Eq. 8) was performed:

$$T(t) = T_0 - qt - \Delta \sin(\omega t). \quad (8)$$

Here T_0 is the initial temperature, q is the cooling rate, Δ is the amplitude of the temperature oscillations, ω is the frequency, and t is the time. We assume that 20 periods of temperature oscillations occur during melt crystallization, which is sufficient to understand the nature of the process, and also corresponds to the order of the number of observed oscillatory zones in natural zircons (e.g., **Fig. 1**).

Figure 7 shows the evolution of the zircon radius (a) and growth rate (b) for the temperature history given by Eq. (8) over the total cooling time (in kyr). The total duration of these numerical experiments ranges from 500 to 50,000 years (corresponding to average cooling rates of 0.25°C/yr to 0.0025°C/yr). It results in a zircon of smaller size at the faster cooling rate, largely because when temperature drops rapidly, the diffusion of Zr in the melt slows and the zircon does not grow as large due to diffusion limitation. For average cooling rates of <0.025°C/yr, zircons grow to a radius of 65-80μm. It is a notable result of our simulations that small to moderate temperature oscillations of several °C do not lead to zircon dissolution at any cooling rates, but instead lead to a decreased growth rates in zircon (**Fig. 7b**). This happens because Zr concentrations in the boundary layer are initially very low in the boundary layer (trough) around the growing crystal. With a T increase, the concentration at the interface $C_{sat}(T)$ starts to increase to a new C_{sat} level corresponding to the increasing temperature. However, the diffusive flux fills the deep

trough making it shallower while the concentration gradient near boundary remains negative, which according to Eq. (2) keeps the zircon growth velocity (*V*) positive, leading to decelerated zircon growth. When the concentration near the boundary becomes flat, zircon growth stops. It is therefore the slow diffusion of Zr that damps (modulates) small *T* oscillations in a melt cell surrounding zircon. We further experimented with a larger ΔT amplitudes of oscillation of ≥10°C and observed that for a 50ky cooling time ΔT needed to be more than 10°C to stop zircon growth ($V = 0$) and begin dissolution during oscillations. In the case of a 0.5 ky cooling time, only during the first two temperature cycles is zircon dissolution observed for the amplitude 10°C of temperature fluctuation. When the temperature drops rapidly to low values, the Zr gradient (**Fig. 4**) in the boundary layer becomes too large to overcome, preventing zircon dissolution during the next temperature increase. Higher temperatures and faster Zr diffusion at higher H_2O_{melt} lead to a shallower trough near the zircon-melt boundary, (Eq. 5, **Fig. 3**). For lower *T* systems with slow Zr diffusivities, lower water, and for quicker cooling times, the concentrational troughs around growing zircons are deeper (**Fig. 4**). For such systems, there is a greater tolerance to stronger ΔT oscillation of 10-20°C of continuing zircon growth without causing zircon dissolution.

There is a progressive decrease in the growth rate as the temperature decreases due to a decrease in Zr supply to the growing crystal as diffusion slows down at lower temperatures. Marked oscillations in the growth rate are caused by changes in the Zr equilibrium concentration with temperature (5 to 10 ppm of Zr in melt for the temperature change $\pm$ 3 ^{o}C). Changes in the Zr concentration at the interface affect the concentration gradient strongly and, as a consequence of the boundary condition (Eq. 2), the growth rate

of the crystal. Stronger oscillations of the growth rates at low cooling rates are caused by the ability of Zr to diffuse in and out of the boundary given longer timescales between oscillations.

3.4. Temperature oscillations effects on Hf and Y partition

Figure 7 (c and d) shows the profile of Hf and Y concentrations in zircon as an example of trace element concentrations in zircon reacting to temperature oscillations. Other elements will show similar but less prominent behavior and are considered in **Fig. 8**. The Hf concentration is low in the boundary layer during periods of rapid zircon growth at any growth rate due to its strong partitioning into zircon (see **Fig. 4**). With each periodic increase in temperature along the cooling path, the growth rate decreases. Thus, the diffusion of Hf from the vicinity of the melt to the boundary layer leads to an increase in the Hf concentration at crystal-melt interface and, following partition relationships, the Hf concentration in the crystal. On the local minima of the ΔT oscillation, the zircon growth rate increases and the Hf content in the boundary layer drops down rapidly to a deep through.

There is also an important difference in the influence of temperature oscillations at different cooling rates as observed in the models over 0.5, 5, 25 and 50 ka for an 840 to 720°C temperature decrease. For faster cooling (840 to 720°C in 0.5 and 5 ka, green and blue curves, **Fig. 7**), zircon crystals are smaller. The supply of Hf to the boundary layer is not efficient because of the slow diffusion at low temperatures and the overall Hf content in the crystal progressively decreases from core to rim (compare with **Fig. 5**) in spite of increase in the partition coefficient. At lower cooling rates, the Hf partition coefficient

increase dominates leading to an overall increase in Hf concentration towards the crystal rim. Natural zircons typically have an increase in Hf concentrations toward the rim (Claiborne et al. 2017) with Zr/Hf ratio of about 1.3. This may indicate that many zircons studied by these authors reflect relatively slow cooling conditions.

At any cooling rates, but more so for slow cooling, Hf oscillatory zoning in zircon is wide in the core (zones of up to 10μm wide) and narrower (~1μm wide) in the rim because zircon growth rates decrease at low temperatures and the amount of growth during one temperature cycle becomes smaller. This effect is independent on the simple radius-volume relationship on decreasing of thickness of growth zones with increasing radius from the center of zircon. This is a common observation in zoning patterns within natural zircons and other accessory minerals in which cores are rather homogenous (and often with sector zoning, also signifying faster growth; Liang and Watson, 1995; **Fig. A2**, supplementary) and rims are finely zoned (**Fig. 1**; Corfu et al., 2003; Hoskin and Schaltegger, 2009).

Furthermore, the shape of the Hf oscillations and concentration profiles in zircon are different in the cases of fast and slow cooling. At slow cooling, higher concentrations of Hf have sharp terminations at inflection points, and at fast cooling rates oscillatory zoning is more sinusoidal and similar to the ΔT vs time function (Eq. 8). These predictions are an important result for current and future imaging efforts of zircon oscillations by either electron microprobe or NanoSIMS (**Fig. 1**, A1, Hoffman et al., 2009) as analytical capabilities to image the shapes of individual oscillations at sub-micron level increases. A prediction from our work is that sharp terminations result from slow but large ΔT variations while smoothed oscillations in trace element concentrations may not necessarily

reflect post-entrapment diffusional relaxation but rather be a prime growth feature at relatively fast (e.g. >0.02°C/yr) cooling rates.

Figure 7d demonstrates the evolution of Y concentrations in zircons for different cooling rates. Y is also an analogue for the behavior of the mid-heavy REEs considered below. Due to fast diffusion and a steeper K_d vs $1/T$ partition dependence (than for Hf, see **Fig. 3**), Y concentration in zircon progressively and dramatically increases to 1.5 wt% from the core to the rim of the modeled zircon (**Fig. 7**) at any studied cooling histories. Furthermore, the faster diffusion of Y (**Fig. 3a**) as compared to Zr and Hf, makes it respond to changes in growth rate more rapidly, and the Y concentration in the crystal more closely reflects the local crystal-melt equilibrium at any given temperature (shallower troughs on **Fig. 4**). Y rim concentration slightly increases with the increase in overall cooling time. Additionally, the resulting oscillations are always more sinusoidal and symmetric than for Hf.

3.5 Temperature oscillation effects on other trace elements

Figures 8a-c demonstrate variations in Hf, Y, U, Th, P and Dy for the same linear cooling over 0.5, 5, 25 and 50 ky from 840 to 720°C as is described in **Fig 7a**. Many observations related to oscillatory zoning patterns (width, amplitude, shape, terminations) for Hf and Y, hold for the other elements as a function of their partition and diffusion relations (**Fig. 3**): elements with slower diffusion (P, Y, U, Th) exhibit a sawtooth pattern of oscillations in contrast to more sinusoidal zoning for other, faster diffusing elements. Also notice that the width of oscillatory zones coincides for all of the elements despite them having rather different (±1 order of magnitude) diffusion coefficients in melt (**Fig.**

3a). This result suggests that oscillations are mostly controlled by the frequency of temperature oscillations and zircon growth rates during each period rather than rates of diffusion of trace elements in the melt. Coeval oscillations of elements are commonly, but not universally observed in natural zircons analyzed and profiled in situ, (**Fig. 1**; Claiborne et al. 2017), and should apply to zircons with simple growth histories.

The overall amplitude of trace elemental fluctuations of the concentrations of other trace elements are significantly smaller in comparison with Hf. The amplitude of oscillations is a function of partition coefficient, where elements with the highest *K* values exhibit stronger amplitude oscillations, shown here for $\Delta = \pm 3°C$ case. In comparison with Hf, all other trace elements have lower partition coefficients. During zircon growth the melt in the vicinity of growing zircon becomes less depleted with U, Th and Dy. With an increase in *K* at lower temperatures (**Fig. 3b**) concentrations of these trace elements in the crystal also increase but to a lesser degree than Y. Overall fluctuations of the concentrations are significantly smaller because of a weaker feedback between the growth rate and trace element partitioning as the system cools.

3.6. Effects of major and other accessory mineral crystallization

Next, we consider the influence of another major, minor, or non-zircon accessory mineral crystallization on the outer cell boundary (**Fig. 2**) on the partitioning of trace elements in zircon in the center of melt cell (**Fig. 8d)**. The crystallization of plagioclase results in melt cell enrichment in Zr and other trace elements because they are incompatible in plagioclase and most other major minerals such as quartz and sanidine. Crystallization of these major minerals, for the same cooling conditions as is shown in

Figs. 7-8, results in a larger zircon crystal by a factor of two (as was shown in Fig. 15 of Bindeman and Melnik, 2016). The present study also demonstrates that the crystal becomes enriched in Hf and other incompatible trace elements relative to a model with no major phase crystallization, as these are pushed into the melt cell surrounding zircon by a major phase.

The core to rim trace elemental concentrations in zircon change dramatically if co-crystallization of minerals with non-negligible *K* for the considered elements is involved, such as sphene (for Y), apatite (for P), monazite (for P and LREEs), chevkinite (REEs), and amphibole (MREEs). For example, if sphene and hornblende crystallization is allowed in addition to plagioclase on the outer boundary of our model set up (**Fig. 2**), Y and Dy concentrations in the melt and in zircon drops because last two of these minerals have high partition coefficients for Y and Dy (Bachmann et al., 2005; PetDb.org). It can be noted, however, that the amplitude of elemental concentration oscillations in zircon for elements not entering sphene or hornblende (e.g. Hf) does not strongly depend on their crystallization (**Fig. 7 c** vs **d**). For elements strongly partitioned into sphene, such as Y, oscillations in zircons are dampened, but still present. This means that the main mechanism responsible for the presence of oscillatory zoning is not the co-crystallization of other minerals, but rather the simple feedback between zircon growth rate and partitioning seen in **Fig 7**.

3.7. Water pressure oscillation effects on elemental partitioning in zircon

Another intensive parameter that has been proposed to cause elemental oscillations most notably in plagioclase is water pressure, which strongly affects melt phase diagrams

(Bowen, 1928; Sibley et a. 1976) (**Figs. 9-10**). However, changes in water pressure do not directly affect the crystallization of accessory minerals and zircon specifically. Nonetheless, the influence of water pressure oscillations in melt surrounding zircon is non-trivial because of its strong influence on Zr and other element diffusion coefficients (Eq. 5) in water-saturated magmas (**Fig. 9a**), especially at low H_2O contents. As the zircon growth rate is governed by the Zr diffusion coefficient, variations of ~0.2 wt% in the water content lead to changes in the value of the Zr diffusion coefficient by up to a factor of 2 in accordance with Eq. 5 and parametrized results from Watson and Harrison (1983) and Zhang et al. (2010). In contrast, simulations reveal that Hf, P and Dy are less sensitive to variations in water content, while U, Th and Y show stronger oscillations with a frequency governed by water content variations.

Fig. 9b shows the results of numerical simulations with simultaneous sinusoidal variations in temperature and water content during cooling. We assume that the temperature has 10 oscillations during cooling (e.g. refills by hotter magmas) while water content oscillates 3 times faster (due to convection, or changes in overpressure due to crack propagation). Trace element partitioning is very different in this case. Hf and Dy are only sensitive to temperature oscillations, while U and Th oscillate at the frequency ofwater content changes. In contrast, two frequencies are clearly seen in P and especially Y. We therefore see that if the X_{H2O}-T path of growing zircons is more complicated the distribution of trace elements can also show patterns that are difficult to interpret.

Oscillatory changes of water concentrations on the order of $\pm$0.1 wt% in melt are easy to achieve during $\pm$35-50 bar pressure oscillations in many shallow, water-saturated magma systems during closed-system degassing (**Fig. 10**). The coexisting gas bubble

serves as a medium and a host for water partitioning as is explained in **Fig. 10b-c**. The magnitude of these pressure oscillations is comparable to less than the overpressure changes suggested by many magma systems and is below the cracking limits of rocks (Costa et al. 2012).

4. Discussion

Numerical experimentation throughout our parameter space confirms our intuitive supposition that oscillatory zoning in zircons cannot be produced by instabilities of boundary layers in respect to monotonic decreases in temperature or water content, crystallization of other minerals nearby, or by interface kinetic reactions such as Y+P=Zr +Si. Zircon has a nearly constant composition and its growth is governed only by the diffusion of Zr towards the crystal. Due to the large zircon-melt partition coefficient of Zr, growth rates of zircon are much slower than those for plagioclase. Thus, local thermodynamic equilibrium is maintained at the zircon-melt interface. All trace elements diffuse independently due to their low concentrations in the melt and there is no competition between them while partitioning into zircon. In contrast, for a major phase such as plagioclase, oscillatory zoning is caused by albite-anorthite partitioning (Morse, 1994) and involves ther diffusion of several competing major elements with different diffusivities. Due to large concentrations in the melt, diffusion of major elements is not independent (e.g. Liang et al. 1994) and for plagioclase is described by a diffusion matrix that is also dependent on water (Gorokhova and Melnik, 2010). With much faster plagioclase growth rates, there is a tight relationship between the growth rate and local

interface undercooling that is itself strongly dependent on the composition of the boundary layer of plagioclase-compatible elements.

Thus, the only way forward to explain pervasive oscillatory zoning of zircon and other accessory minerals is by variations in external intensive parameters: temperature, and for water saturated magmas only, pressure fluctuations, which affects water content-dependent diffusivities in the melt. We demonstrated that small temperature oscillations of only few degrees C can lead to significant variations in Hf and other element content within zircons (**Figs. 7-9**).

Our modeling demonstrates that if temperature oscillations are small and frequently spaced along the overall cooling path, oscillatory temperature increases of small magnitude will not lead to zircon dissolution. Small temperature increases of several °C will only temporarily slow down or suspend zircon growth (**Fig. 7**). New layers of zircon will partition trace elements from the immediate boundary layer (**Fig. 4**) in which elements with different diffusivities and partition coefficients will react to zircon boundary advance kinetics, thus recording oscillating temperatures in accordance with each element partition and diffusion coefficient. Our numerical model fundamentally shows that variations in these three parameters: diffusion, partition coefficients, and rate of growth are sufficient to explain the observed features of coeval oscillating elemental variations and predicts that these are to be of similar wavelengths but different amplitude.

More prominent oscillations of greater than ±10°C will lead to zircon dissolution and recycling of the outer boundary of zircon, but as is outlined above cannot be modeled within the framework of our model. Such phenomena are abundant in nature (e.g. the outer zone on **Fig. 1**; Corfu et al., 2003; Hoskin and Schaltegger, 2003) and are easily

recognized by truncated growth boundaries, truncating concentric oscillatory zoning. Our modeling however may put upper limits on the possible temperature oscillations in "simple" zircons in nature of approximately less than 10°C. This suggests that their textural examination by cathodoluminescence and trace element profiling with high spatial resolution can be used to prove their single cooling (± ΔT) origin.

Our model does not consider non-equilibrium zircon partitioning related to non-trivial Henry's law constant variations with concentration and temperature (Whitehouse and Kamber, 2002; Hoskin and Schaltegger, 2009). However, we consider that even if present, the above relationships are likely smooth and continuous with temperature and concentration, and cannot be the origin of oscillations, however they can perhaps increase or decrease the amplitudes in proportion to the activity coefficient (γ) variations with concentration ($a=\gamma*C$), and thus K. The main conclusion of the present work is that the simplest model of temperature oscillation of ±3 to 10°C is already adequate to explain the factor of ~2 variations in trace element concentrations within zones as well as the width of those zoning patterns (e.g., **Fig. 1**).

Another interesting result of our modeling is that prescribed (Eq. 8) temperature, and/or water content oscillations generate rather smooth oscillatory growth zoning (**Figs. 7-9**). Similarly, smoothed (not abrupt or step-function) zoning patterns are found in many natural zircons, and may not necessarily require post-growth intracrystalline diffusion. Step-function zoning is commonly assumed to be a result of "rapid" crystallization following dissolution, and is commonly assumed as an initial condition for interdiffusion between adjacent zones in crystals, used in geospidometry and crystal residence studies.

Instead, we find that these patterns may result from precisely the opposite: a system with slow zircon growth driven by slow cooling rates in a large pluton.

5. Implications for magmatic systems

Small temperature variations could be a consequence of convection in large and slowly cooling magmatic bodies, and oscillatory zoning in crystals has traditionally been interpreted to reflect such processes. Bowen (1928) suggested that oscillatory zoning in plagioclase may be related to convection in the magma chamber whereby each crystal travels through a diversity of temperatures and pressures in a cyclical fashion, a model which remains popular today. As crystals may have different trajectories in temperature, time, and space before being assembled by magma mixing into a single hand specimen, zoning patterns of neighboring crystals may differ. **Figure 10** presents a cartoon view of a magma chamber with mushy and liquid parts that may experience of temperature and pressure increases due to replenishments by hotter magmas from below causing compositional and thermal convection, which may also affect the P-T condition experienced by any given crystal.

Besides variations in temperature, oscillations in fluid pressure have long been called upon to explain plagioclase zoning (Bowen, 1928; Morse, 1994), but such effects will not directly be applicable to zircon and other accessory phases as these do not affect saturation and partitioning relations (**Fig. 3b**). However, as we demonstrated above, variations in fluid pressure affect zircon oscillatory zoning comes in a less trivial way via oscillations of X_{H2O} in the melt surrounding the zircon, which affects the diffusion coefficients of Zr and other trace elements. This water effect is stronger at low water

concentrations as the effect of water on diffusion is the strongest for the first 0.3 wt% increase in water compared to s subsequent 3 wt% water increase (Watson and Harrison, 1983).

This control by water is possible only for water-saturated shallow magma bodies (gas bubble in **Fig. 11b**), where external pressure variations are transmitted to water concentrations in melt causing water to diffuse in and out of gas bubbles. For example, magma bodies located in the shallow crust a few kilometers deep (equivalent to 0.3-0.5 kbar pressure) will be water saturated with C_{H2O} between 2-3wt% (Newman and Lowenstern, 2002).

Many shallow magma bodies, including the Bishop and Fish Canyon Tuffs were likely water-saturated (Anderson et al. 2000; Bachmann et al. 2002). Such compressible magma bodies are capable of sustaining pressure variations on the order of $\pm$35-50 bars due to: rejuvenation, eruptions, dike formation, and perhaps external tectonic forces as is portrayed in **Fig. 11**. Pressure increases followed by thermal and viscous relaxation will cause water to migrate in and out of gas bubble a melt cell, in turn causing the zircon to develop oscillations. Coupled temperature and pressure oscillations of different frequencies (**Figs. 9-10**) will cause non-monotonic oscillations of different wavelengths, which will be variable for each element. For water-saturated or undersaturated magma bodies an alternative scenario may involve H_2O and CO_2 fluxing of more static magma mushes, causing variations in X_{H2O}.

Our modeling confirms that prominent oscillatory zoning should characterize near-solidus ~700°C plutonic and mush-related zircons, commonly from cold and wet environments as compared to >800°C hot and dry, water-saturated rhyolites, which show

more subdued oscillatory zoning (e.g., **Fig. 1, Fig A1** supplementary, Claiborne et al., 2010 vs. Carley et al. 2011). To illustrate this point, our imaging of the trace element distribution in zircons from Fish Canyon tuff (cold, ~750°C), Toba (hotter, ~780°C), and Yellowstone (hot, ~850°C) systems (Loewen and Bindeman, 2016, **Figs. 1, A1**) supports this point. The example for the cold system is the Spirit Mountain Batholith studied by Claiborne et al. (2010) which has cores are not zoned while the rims have oscillatory zoning, in line with our **Fig. 8-9**. Hot Icelandic rhyolites (Carley et al. 2011) are similar to Yellowstone-Snake River Plain rhyolites in dull cathodoluminesence images and a lack of oscillations (e.g. Watts et al., 2012; Colón et al. 2015).

Temperature fluctuations may be the result of pluton formation by multiple dike-sill injections (Annen et al. 2006), and our companion paper modeled these effects on zircon growth and dissolution (Bindeman and Melnik, 2016). We observed that with an increase in distance from a sill injection zone, the amplitude of temperature disturbances in a zircon-bearing parcel of magma or rock will progressively decrease along with the sharpness of the temperature fronts. This will result in less pronounced oscillatory zones towards the rim of zircons away from the oscillating heat source ("hot zone").

Finally, our modeling provides some instruction for rapidly improving in situ analysis of zircons with micron to submicron spatial resolution. The scale of zoning that we recover from our modeling ranges from 1 to 10 μm (**Fig 7-9**) and the amplitude of variation is less than a factor of two. Therefore, our modeling provides guiding principles for modern methods for zircon microanalysis. Such studies should therefore provide adequate characterization of the evolution of magmatic systems using the accessory minerals.

Acknowledgements. OEM acknowledge support from the Russian Foundation for Basic Research (RFBR, grant number 15-01-02639), and the University of Oregon Meierjurgen and Global Oregon Faculty Collaboration Fund for funding this research. INB Acknowledges support from NSF grant 1447337. We thank Dylan Colón and Mike Hudak for edits and comments, Calvin Miller, and two anonymous reviewers for reviews, and Renat Almeev and Keith Putirka for editorial comments.

REFERENCES

Annen, C., Blundy, J.D., Sparks, and R.S.J. (2006) The genesis of intermediate and silicic magmas in deep crustal hot zones. Journal of Petrology 47 (3), 505-539

Aranovich, L. Ya., Bortnikov N.S., T. F. Zinger, S. E. Borisovskiy, V. A. Matrenichev, A. N. Pertsev, E. V. Sharkov, and S. G. Skolotnev (2018). Morphology and Impurity Elements of Zircon in the Oceanic Lithosphere at the Mid-Atlantic Ridge Axial Zone (6°–13° N): Evidence of Specifics of Magmatic Crystallization and Postmagmatic Transformations Petrology, 2017, Vol. 25, No. 4, pp. 339–364.

Bacon, C.R. (1989) Crystallization of accessory phases in magmas by local saturation adjacent to phenocrysts. Geochimica et Cosmochimica Acta 53 (5), 1055-1066.

Bachmann, O., Dungan, M. A. & Lipman, P. W. (2002). The Fish Canyon magma body, San Juan volcanic field, Colorado: Rejuvenation and eruption of an upper crustal batholith. Journal of Petrology 43, 1469–1503.

Bachmann, O., Dungan, M. A., & Bussy, F. (2005). Insights into shallow magmatic processes in large silicic magma bodies: The trace element record in the fish canyon magma body, Colorado. Contributions to Mineralogy and Petrology,

149(3), 338-349. doi:http://dx.doi.org/10.1007/s00410-005-0653-z

Bindeman, I.N., and Melnik, O.E. (2016) Zircon survival, rebirth and recycling during crustal melting, magma crystallization, and mixing based on numerical modelling. Journal of Petrology, 57, 437-460.

Boehnke, P., Watson, E.B., Trail, D., Harrison, T.M., and Schmitt, A.K. (2013) Zircon saturation re-revisited. Chemical Geology 351, 324-334.

Bowen, N.L. (1928) The Evolution of the lgneous Rocks. 334 p., Princeton Univ. press, Princeton, New Jersey.

Bunsen R.W. (1851) Über die Processe der volkanischen Gesteinsbildungen Islands. Annual Review of Physical Chemistry, 83,197–272.

Carley T.L., Miller C.F., Wooden J.L., Bindeman I.N., and Barth A.P. (2011) Zircon from historic eruptions in Iceland: Reconstructing storage and evolution of silicic magmas: Mineralogy and Petrology, 102, 135-161.

Cherniak D.J., Hanchar J.M., and Watson E.B. (1997a) Rare-Earth diffusion in zircon. Chemical Geology, 134, 289–301

Cherniak D.J., Hanchar J.M., and Watson E.B. (1997b) Diffusion of tetravalent cations in zircon. Contribution to Mineralogy and Petrology, 127,383–390

Claiborne L.L., Miller C.F., Gualda G.A.R., Carley T.L. Covey A.K. Wooden J.L. and Fleming M.A. (2017) Zircon as magma monitor: Robust, temperature-dependent partition coefficients from glass and zircon surface and rim measurements from natural systems. AGU Book series, accepted

Claiborne, L.L., Miller, C.F., and Wooden, J.L. (2010) Trace element composition of igneous zircon: a thermal and compositional record of the accumulation and

evolution of a large silicic batholith, Spirit Mountain, Nevada. Contributions to Mineralogy and Petrology, 160, 511.

Colón, D.P., Bindeman, I.N., Ellis, B.S., Schmitt, A.K., and Fisher, C.M. (2015) Hydrothermal alteration and melting of the crust during the Columbia River Basalt-Snake River Plain transition and the origin of low-δ18O rhyolites of the central Snake River Plain. Lithos, 224-225: 310-323

Corfu, F. , Hanchar, J.M., Hoskin, P.W.O., and Kinny, P. (2003) Atlas of zircon textures. in Zircon, Reviews in Mineralogy and Geochemistry, 53 (1), 469-500,

Costa, F., Chakraborty, S., Dohmen, R. (2003) Diffusion coupling between trace and major elements and a model for calculation of magma residence times using plagioclase. Geochimica et Cosmochimica Acta, 67, 2189–2200.

Crowley, J.L., and Bowring S.A. Hanchar J.M. (2006) What is a magma crystallization age? Insight from micro-sampling of chemical domains in zircon from the Fish Canyon Tuff. GCA 10.1016/j.gca.2006.06.153

De Hoog J.C.M., Lissenberg C.J., Brooker R.A., Hinton R., Trail D., Hellebrand E.W.G., and Brooker R.A. (2014) Hydrogen incorporation and charge balance in natural zircon. Geochimica et Cosmochimica Acta, 141, 472–486.

Finch, R.J., Hanchar, J.M., Hoskin, P.W.O., and Burns P.C. (2001) Rare-earth elements in synthetic zircon: Part 2. A single-crystal X-ray study of xenotime substitution . American Mineralogist, 86, 681–689.

Fu B., F. Page Z., Cavosie A.,. Fournelle, J. Kita, N., Lackey J.S., Wilde S., and Valley, J.W. (2008) Ti-in-zircon thermometry: applications and limitations. Contributions to Mineralogy and Petrology, 156, 197–215.

Ghiorso M. S. and Sack R.O. (1995). Chemical mass-transfer in magmatic processes IV: A revised and internally-consistent thermodynamic model for the interpolation and extrapolation of liquid–solid equilibria in magmatic systems at elevated temperatures and pressures. Contributions to Mineralogy and Petrology 119, 197–212.

Gorokhova N.V. and Melnik O. (2010) Modeling of the dynamics of diffusion crystal Hahn,M., Behrens H., Tegge-Schüring A., Koepke J., Horn I., Rickers K., Falkenberg G. and Wiedenbeck M. (2005) Trace element diffusion in rhyolitic melts: comparison between synchrotron radiation X-ray fluorescence microanalysis (μ-SRXRF) and secondary ion mass spectrometry (SIMS). Eur. J. Min. 17: 233-242.

Hanchar J.M., and van Westrenen W. (2007) Rare Earth Element Behavior in Zircon-Melt Systems. ELEMENTS, 3(1), 37-42.

Hanchar, J.M., Finch, R.J., Hoskin, P.W.O., Watson, E.B., Cherniak, D.J., and Mariano, A.N. (2001) Rare earth elements in synthetic zircon. 1. Synthesis and rare earth element and phosphorus doping. American Mineralogist, 86, 667-680.

Harrison, T.M., and Watson, E.B. (1984) The behavior of apatite during crustal anatexis: equilibrium and kinetic considerations. Geochimica et Cosmochimica Acta, 48 (7), 1467-1477.

Harrison, T.M., and Watson, E.B. (1983) Kinetics of zircon dissolution and zirconium diffusion in granitic melts of variable water content. Contributions to Mineralogy and Petrology, 84, 66-72.

Hofmann A.E., Valley JW, Watson E.B., Cavosie A.J., and Eiler J.M. (2009) Sub-micron scale distributions of trace elements in zircon. Contributions to Mineralogy and Petrology, 158, 317–335.

Hoskin, P.W.O. and Schaltegger, U. (2003) The composition of zircon and igneous and metamorphic petrogenesis. In: Hanchar JM, Hoskin PWO (eds) Zircon. Reviews in Mineralogy and Geochemistry, 53, 27–62.

Hayden L.A. and Watson E.B. (2007) Rutile saturation in hydrous siliceous melts and its bearing on Ti-thermometry of quartz and zircon. Earth and Planetary Science Letters, 258, 561–568.

Lasaga, A.C.(1982). Towards a master equation in crystal growth. American Journal of Science, 282, 1264-1288.

Lipman, P.W. (2007) Incremental assembly and prolonged consolidation of Cordilleran magma chambers: Geosphere, v. 3, p. 42–70, doi:10.1130/GES00061.1.

Loewen M.W., Bindeman I.N. (2016) Oxygen isotope thermometry reveals high magmatic temperatures and petrogenetic differences between hot-dry Yellowstone/ Snake River Plain and Icelandic rhyolites compared to cold-wet systems. American Mineralogist, 101, 1222-1227. DOI: 10.2138/am-2016-5591

Loewen M., Bindeman I.N., Melnik O. (2016) Eruption mechanisms and short duration of large rhyolitic lava flows of Yellowstone. *Earth and Planet Sci Lett*, DOI: 10.1016/j.epsl.2016.10.034

L'Heureux,I. (1993) Oscillatory zoning in crystal growth: a constitutional undercooling mechanism. Physical Review E, 48, 4460-4469.

Marshall, D.J. (1988) Catholuminescence of Geological Materials. 146 p., Unwin Hyman,. Boston, London, Sydney,. Wellington.

Morse SA (1994) Basalts and Phase Diagrams: An Introduction to the Quantitative Use of Phase Diagrams in Igneous Petrology, Krieger Publishing Company, 493 pages

Neogi S. Edward W. Bolton E.W., Chakraborty S. (2014)Timescales of disequilibrium melting in the crust: constraints from modelling the distribution of multiple trace elements and a case study from the Lesser Himalayan rocks of Sikkim. Contrib. Mineral Petrol. 168: 1-22, 10.1007/s00410-014-1020-8

Mungall, J. Dingwell, D.B. and Chaussidon, M. (1999) Chemical diffusivities of 18 trace elements in granitoid melts. Geochimica et Cosmochimica Acta, 63, 2599-2610.

Piwinskii, A. J. (1968) Experimental studies of igneous rock series: Central Sierra Nevada Batholith, California. Journal of Geology, 76, 548-570.

Rubatto, D. and Hermann, J. (2007) Experimental zircon/melt and zircon/garnet trace element partitioning and implications for the geochronology of crustal rocks. Chemical Geology, 241, 38–61.

Rustad, J. (2015) Interaction of rhyolite melts with monazite, xenotime and zircon surfaces. Contributions to Mineralogy and Petrology, 169 ,50–58.

Sano Y., Terada K., and Fukuoka T. (2002) High mass resolution ion microprobe analysis of rare earth elements in silicate glass, apatite and zircon: lack of matrix dependency. Chemical Geology, 184 (3), 217-230

Shore, M. and Fowler, A.D. (1996) Oscillatory zoning in minerals: A common phenomenon. Canadian Mineralogist, 34, 1111-1126.

Sibley, D.F., Vogel, T.A., Walker, B.M. and Byerly, G. (1976) The origin of oscillatory zoning in plagioclase: a diffusion and growth controlled model. American Journal of Science, l6, 275-284.

Sparks, R.S.J., and Cashman K.V. (2017) Dynamic Magma Systems: Implications for Forecasting Volcanic Activity Elements, 13, p. 35-40. DOI: 10.2113/gselements.13.1.35

Trail, D., Cherniak, D.J., Watson, E.B., Harrison, T.M. , Weiss, B.P., and Szumila, I. (2016) Li zoning in zircon as a potential geospeedometer and peak temperature indicator. Contributions to Mineralogy and Petrology,171,25.

Vance J.A. (1962) Zoning in igneous plagioclase: normal and oscillatory zoning. American Journal of Science, 260,746–760.

Wallace, G. S. and Bergantz, G. W. (2002) Wavelet based correlation (WBC) of zoned crystal populations and magma mixing, Earth and Planetary Science Letters, 202, 133-145.

Watson, E. B., and Liang, Y. (1995) A simple model for sector zoning in slowly grown crystals: Implications for growth rate and lattice diffusion, with emphasis on accessory minerals in crustal rocks. American Mineralogist, 80(11-12), 1179-1187.

Watson, E.B., and Muller, T. (2009) Non-equilibrium isotopic and elemental fractionation during diffusion-controlled crystal growth under static and dynamic conditions. Chemical Geology, 267, 111-124.

Watson E.B. (1996) Surface enrichment and trace-element uptake during crystal growth. Geochimica et Cosmochimica Acta, **60**, 5013-5020.

Watson, E.B. (1980) Some experimentally-determined zircon/liquid partition coefficients for the rare earth elements. Geochimica et Cosmochimica Acta, 44, 895-897.

Watson, E.B. and Harrison, T.M. (1983) Zircon saturation revisited: temperature and compositional effects in a variety of crustal magma types. Earth and Planetary Science Letters, 64, 295-304.

Watson, E.B., D.A. Wark, and Thomas, J.B.(2006) Crystallization thermometers for zircon and rutile. Contribution to Mineralogy and Petrology, 151, 413-433.

Watts, K.E., Bindeman, I.N. and Schmitt, A.K. (2012) Crystal-scale anatomy of a dying supervolcano: An isotope and geochronology study of individual phenocrysts from voluminous rhyolites of the Yellowstone caldera. Contributions to Mineralogy and Petrology, 164, 45-67

Whitehouse M.J., and Kamber B.S. (2002) On the overabundance of light earth elements in terrestrial zircons and its implication for Earth's earliest magmatic differentiation. Earth and Planetary Science Letters, 204,333-346

Wiebe, R.A. (1968) Plagioclases stratigraphy: record of magmatic conditions and events in a granitic stock. American Journal of Science, 266, 690-703.

Zhang, Y.X., Ni, H., and Chen, Y. (2010) Diffusion data in silicate melts. in: Zhang Y., Cherniak D.J. (Eds), Diffusion in minerals and melts. Reviews in Mineralogy and Geochemistry, 72, 313-408.

Fig. Captions

Fig. 1 Cathodoluminescence (CL) image and trace element profiles through a zircon crystal in Early Fish Canyon Tuff. Profile is from the rim to the core. Dark areas in the CL image dark areas generally correspond to higher concentrations of trace elements. The magnitude of oscillatory zoning is within a factor of two. To a first order there are correlations between greyscales and changes in concentrations. Large increases in Y and P concentrations likely reflect the co-crystallization and dissolution of sphene and apatite that are present in the assemblage. The total number of zones is 20-25 reflecting episodes of thermal perturbation. Data collected on a Cameca 100 Electron microprobe by John Donovan (University of Oregon) using 100 kV voltage, 400 nA current, and collections in four detectors. Beam diameter is 1-2 μm, detection limits are 0.001-0.006 wt%, relative error for each data point is ~2-5%, and the lowest concentrations of P are close to the detection limit.

Fig 2. Model set up with two moving boundaries. Upon cooling, zircon grows at a rate V determined by the saturation conditions and the rate of temperature change. Local thermodynamic equilibrium is assumed. The concentration of Zr (C_{Zr}) at the crystal-melt interface is a function of temperature, while the concentrations of trace elements (C_{tr}) are governed by the zircon-melt partition coefficients K. The crystallization of melt around the zircon at rate W may partition elements in accordance with the bulk partition coefficient k. This will lead to either an enrichment or depletion wave in the melt cell that propagates towards the growing zircon. The melt cell has a T-X phase diagram defined by the user, and it determines the rate W of melt cell expansion or contraction as a function of

temperature and time. C and C_X are the concentration of Zr and trace element in the melt and major minerals, respectively.

Fig. 3 Model input parameters, diffusion and partition coefficients. **(a)** Compilation of diffusion coefficients of relevant elements in a metaluminous rhyolitic melt, shown here for 3 wt.% water following sources cited in Zhang et al. (2010), the parametrization of T and X_{H2O} is given in Eq. 5a in the text. **(b)** Trace element partitioning coefficients as a function of temperature, most data is compiled from Rubatto and Hermann (2007) and checked against the natural data of Claiborne et al. (2017). For Zr saturation Eq. 5b is used. Expressions for trace element diffusion and partition coefficients can be found in the supplementary MATLAB code (functions TraceDiff and Kdd, respectively).

Fig 4. Trace element profiles in melt surrounding a growing zircon crystal after 5000 years of linear cooling from 840°C to 720°C in a melt cell with a radius 2 mm. Notice variable amplitudes of depletion of the boundary layer around zircon for the indicated trace elements, the width and the level of depletion is a function of both the diffusion coefficient and the partition coefficient. Slower diffusion and a high partition coefficient (e.g. Hf) expectedly generates the widest and deepest depletion (e.g. Hf), while fast diffusion (Y, Dy), and/or a smaller partition coefficient (P) generates a narrower boundary layer. Elements are normalized to their far-field concentration in the melt.

Fig 5. Trace element concentration profiles in zircon after a linear cooling from 840° to 720°C over 5000 years in a melt cell with a radius 2 mm and without co-crystallization of other minerals on the outer boundary of the cell. Smooth changes of concentrations are determined by partition coefficients and by the rate of zircon growth. Slower cooling of zircon generates different concentration profiles and levels of enrichment/depletion. In

particular, Hf concentration in zircon increases with slower cooling (see also **Fig. 7** below).

Fig. 6. Normalized concentration of xenotime, YPO_4, in zircon as a function of zircon radius for a linear temperature drop and different values of the xenotime partition coefficient, K_X, assuming no independent partitioning of P and Y into zircon ($K_P = K_Y = 0$). Decreases in xenotime concentration in zircon are primarily controlled by decreases in Y in the boundary layer, while P remains nearly constant in the vicinity of the crystal-melt interface (**Fig. 4**). Notice the lack of oscillations due to the xenotime substitution mechanism.

Fig. 7. Effects of temperature oscillations of ±3°C superimposed on cooling of different rates and duration. Cell size radius is 2 mm. **(a)** Zircon radius, **(b)** growth rate, **(c)** Hf and **(d)** Y concentrations. The legend in **(a)** applies to all graphs and gives the total length of cooling from 840 to 720°C in kyr. Notice that 3°C temperature increases do not cause zircon dissolution but slow down zircon growth **(a, b)**, that the amplitude and width of oscillations is better pronounced for the longer duration of cooling in **(c and d)**, and that faster cooling promotes decreases in Hf concentrations while slow cooling results in a core to rim increases in Hf concentrations, see text for discussion.

Fig. 8 Concentrations of trace elements vs zircon radius at ±3°C for various cooing rates and crystallization scenarios. Cooling is linear from 840°C to 720°C for 0.5, 5, and 50 kyr **(a-c)** with ±3°C sinusoidal temperature oscillations as in **Fig. 7a**. In a-c, melt is crystallizing only zircon. **(d)** Influence of amphibole and sphene co-crystallization on the outer cell boundary (**Fig. 2**) leading to decreases in Y and Dy concentrations in zircon.

Fig. 9a. Concentration of trace elements vs zircon radius with water content oscillations. The latter can be result of the convection of a zircon+bubble melt pocket, pressure oscillations, and H_2O and CO_2 fluxing as is explained in **Fig. 10. (a**) Monotonic cooling is from 840°C to 720°C for 5 kyr with water content oscillation of 3±0.1 wt%. **(b)** The same as **Fig. 9a** but with sinusoidal temperature and water content variations and with the frequency of water content variation of 3 times faster than the temperature oscillations for the temperature. Notice that the width and amplitude of the oscillatory zones becomes decoupled for different elements as a function of their diffusivities at different water content, and partitioning relations.

Fig 10. Cartoon explaining possible causes of temperature and water content oscillations in a water-saturated melt ($P_{total} = P_{H2O}$) surrounding zircon, affecting its growth and partitioning relations (**Fig. 9**). **(a)** Magma chamber that can sustain ΔP pressure oscillations of 50 bar without eruption due to recharge from below and dike formation from above; convection of 150 m in the vertical dimension (±ρgh) is additionally capable of 50 bar pressure variations. **(b)** Zircon, plagioclase and a gas bubble within a melt cell with externally controlled pressure affecting water solubility in the melt and the diffusion of Zr and other trace elements. **(c)** Effects of 35-50 bar pressure oscillations on water content in the melt during closed system degassing into an internal bubble, calculated in VolatiteCalc (Newman and Lowenstern, 2002).

This is a preprint, the final version is subject to change, of the American Mineralogist (MSA)
Cite as Authors (Year) Title. American Mineralogist, in press.
DOI: http://dx.doi.org/10.2138/am-2018-6182

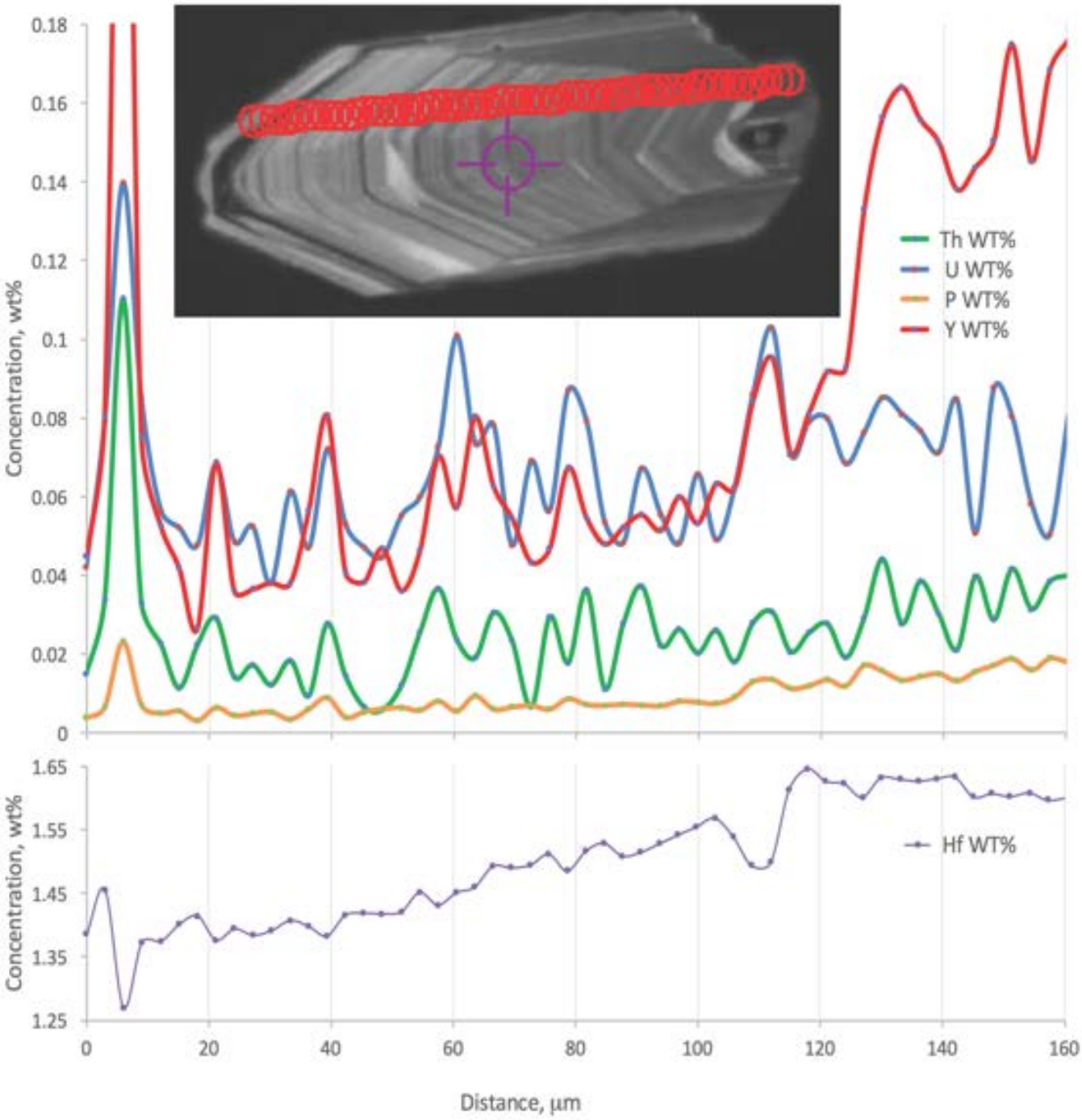

This is a preprint, the final version is subject to change, of the American Mineralogist (MSA)
Cite as Authors (Year) Title. American Mineralogist, in press.
DOI: http://dx.doi.org/10.2138/am-2018-6182

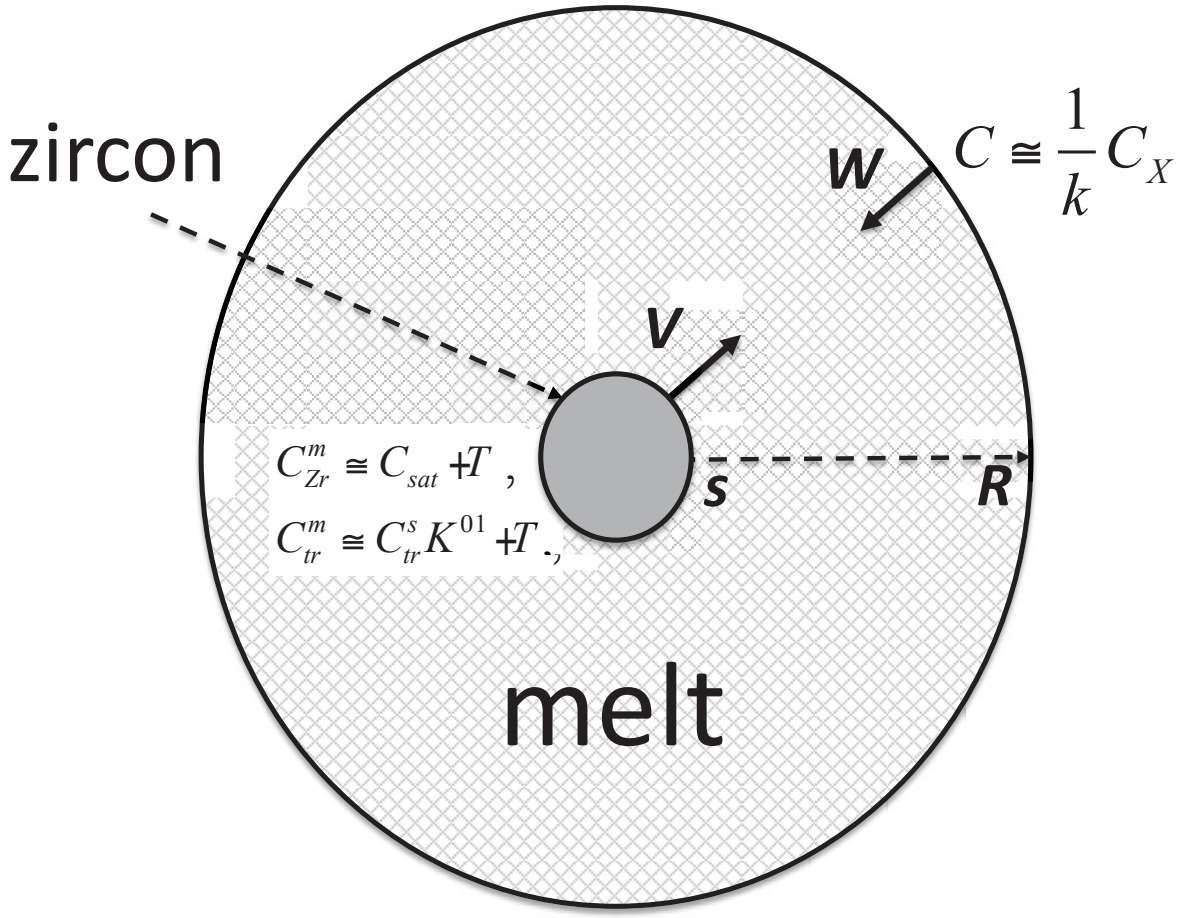

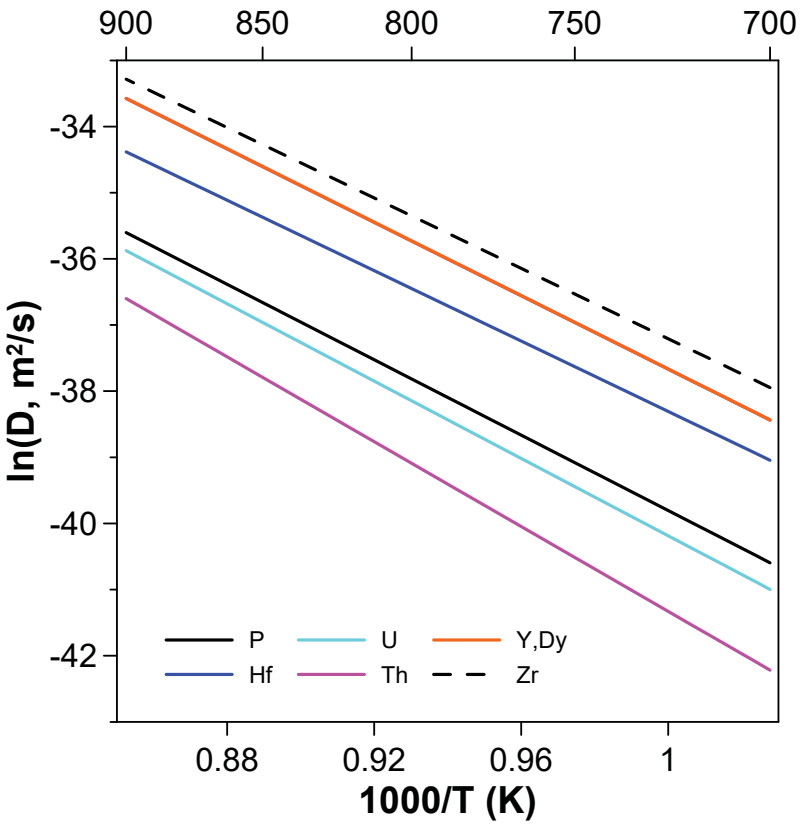
900
850
800
750
700
-34
-36
-38
-40
-42
ln(D, m²/s)
P
Hf
U
Th
Y,Dy
Zr
0.88
0.92
0.96
1
1000/T (K)

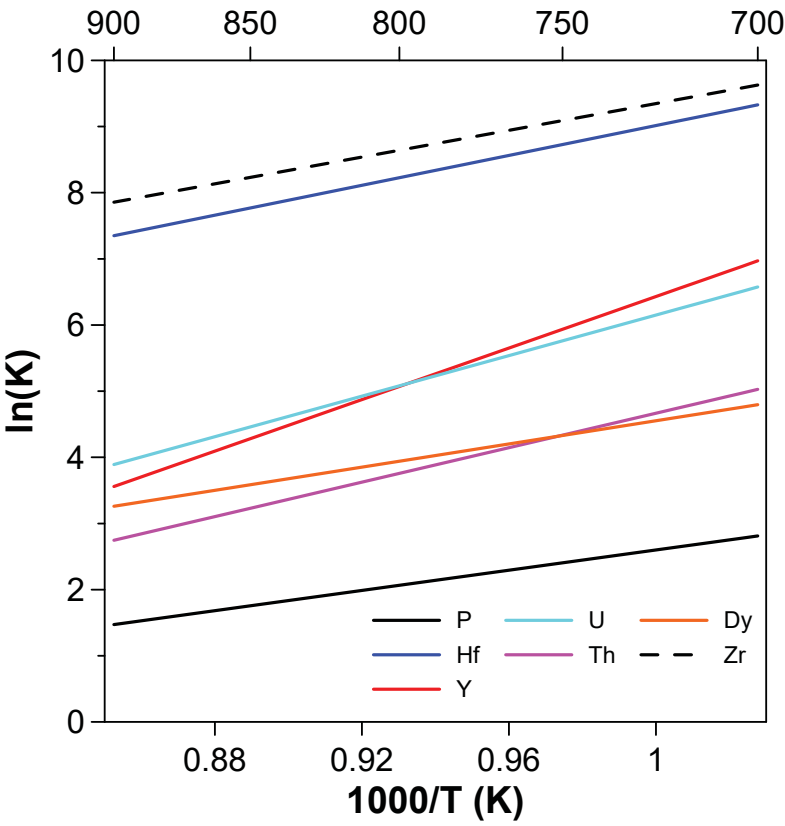
900
850
800
750
700
10
8
6
4
2
0
ln(K)
P
Hf
Y
U
Th
Dy
Zr
0.88
0.92
0.96
1
1000/T (K)

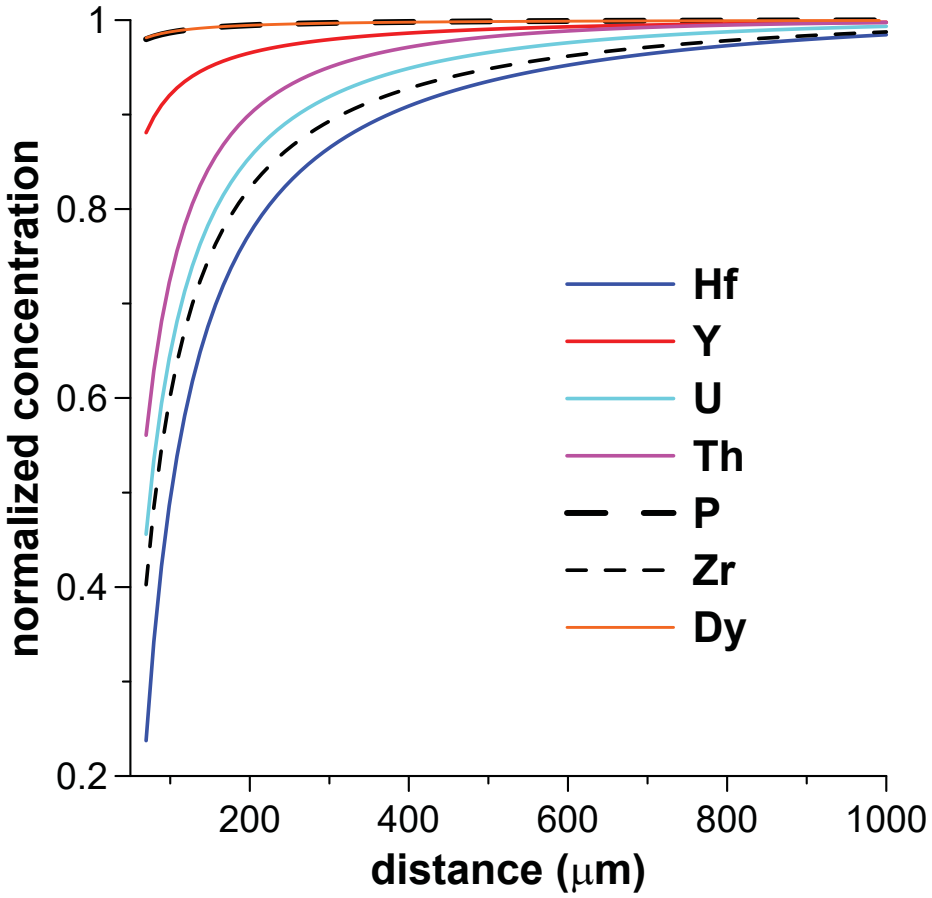
normalized concentration
1
0.8
0.6
0.4
0.2
200
400
600
800
1000
distance (μm)
Hf
Y
U
Th
P
Zr
Dy

This is a preprint, the final version is subject to change, of the American Mineralogist (MSA)
Cite as Authors (Year) Title. American Mineralogist, in press.
DOI: http://dx.doi.org/10.2138/am-2018-6182

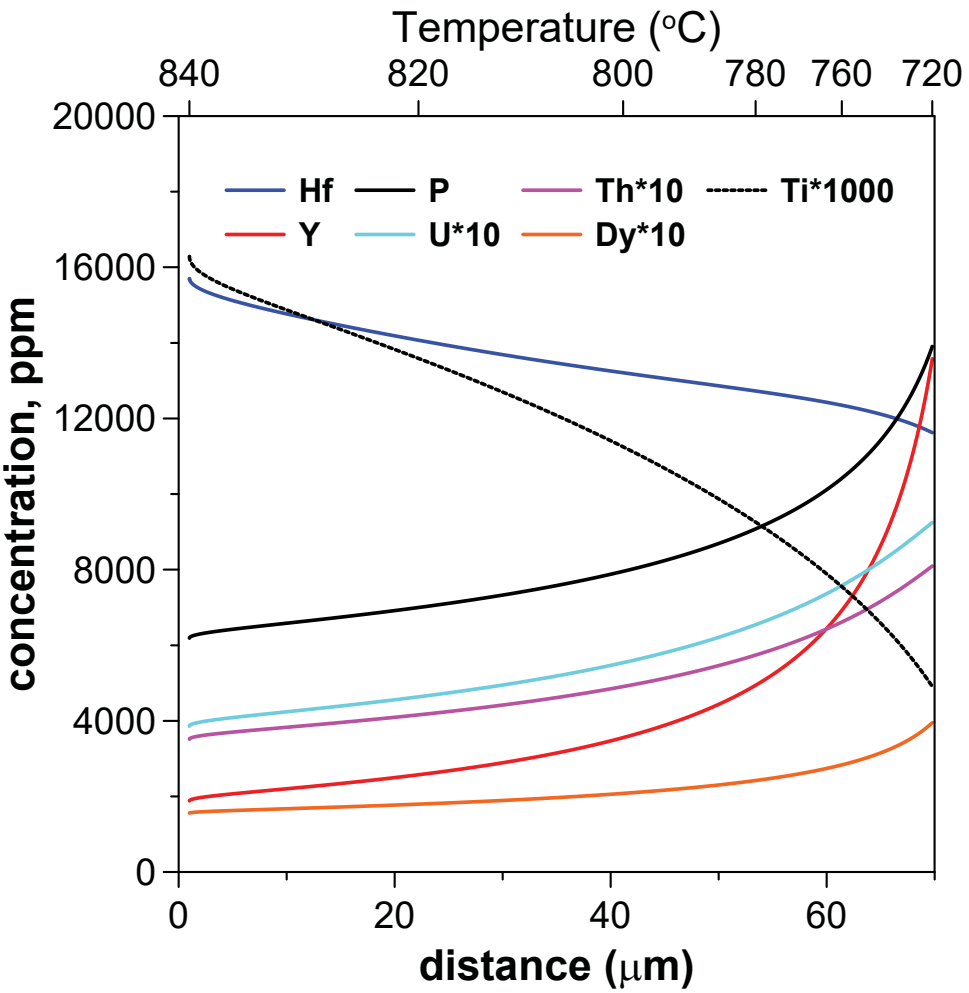

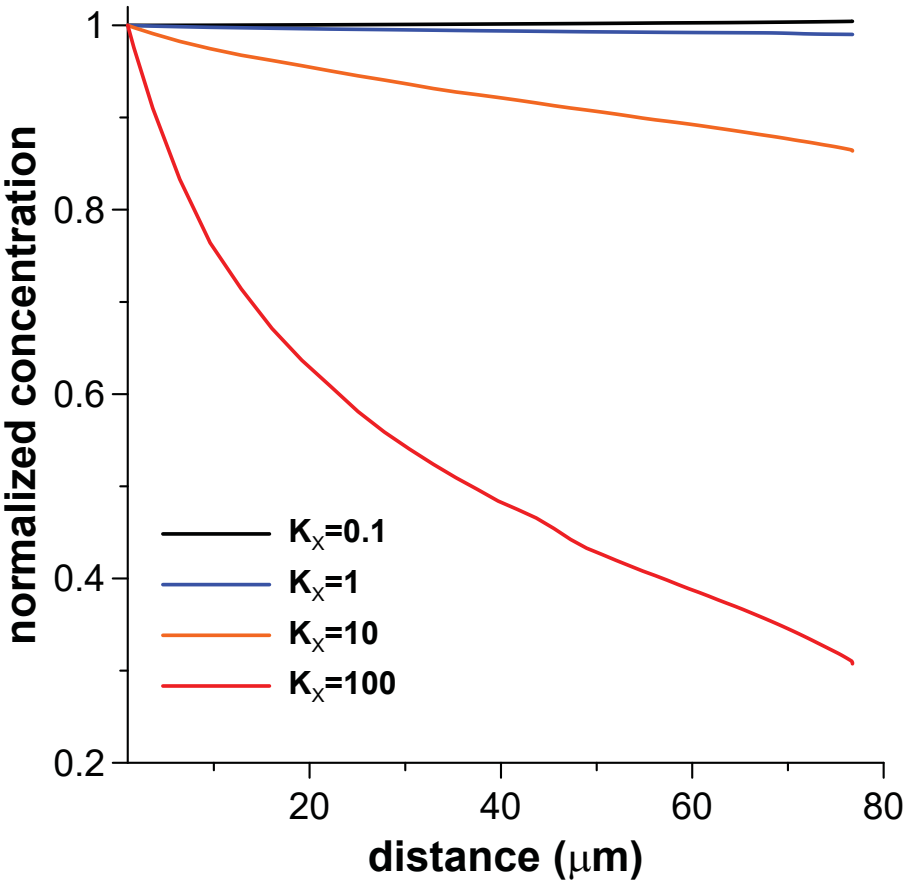
normalized concentration
1
0.8
0.6
0.4
0.2
20
40
60
80
distance (μm)
Kx=0.1
Kx=1
Kx=10
Kx=100

This is a preprint, the final version is subject to change, of the American Mineralogist (MSA)
Cite as Authors (Year) Title. American Mineralogist, in press.
DOI: http://dx.doi.org/10.2138/am-2018-6182

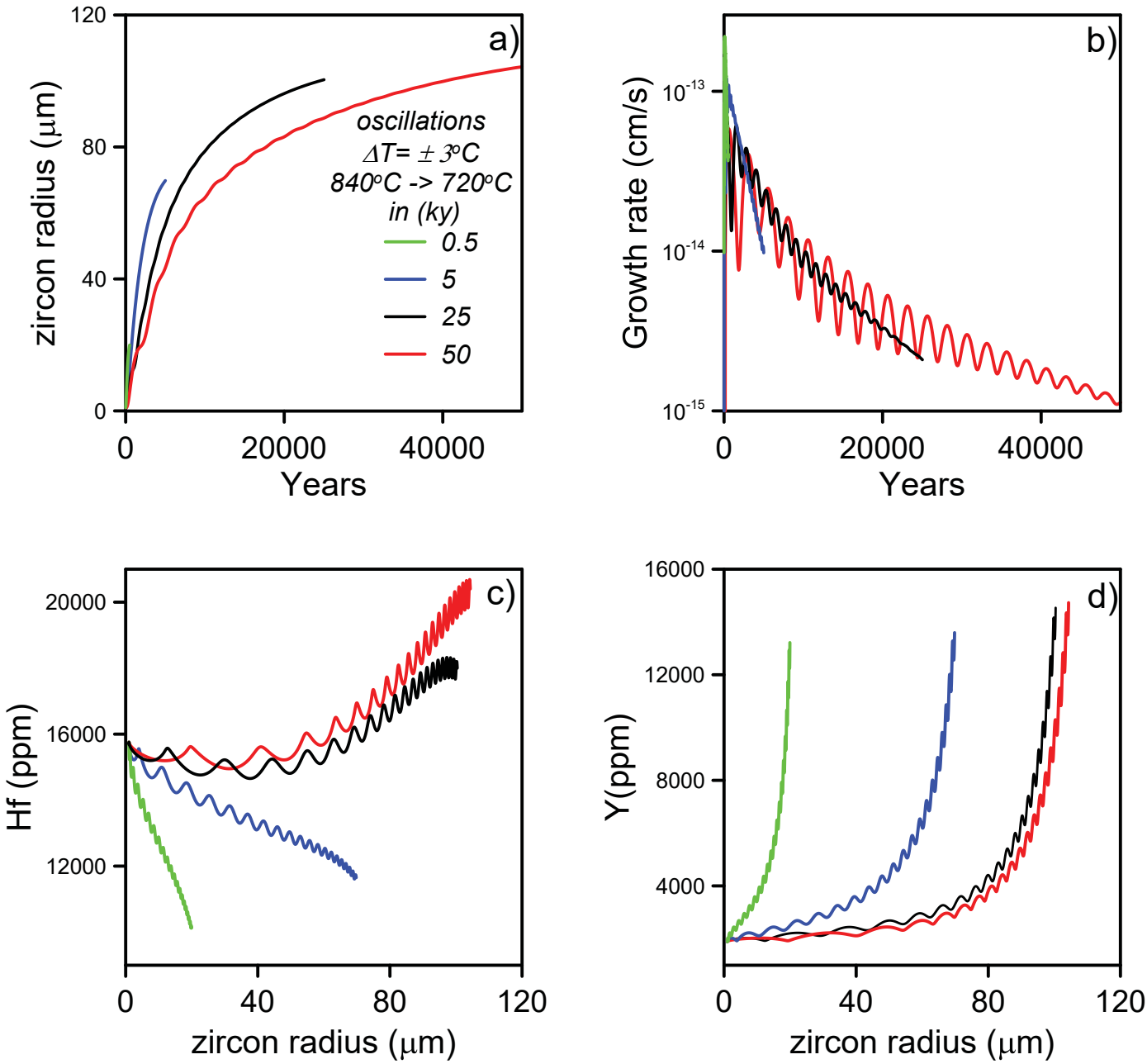

This is a preprint, the final version is subject to change, of the American Mineralogist (MSA)
Cite as Authors (Year) Title. American Mineralogist, in press.
DOI: http://dx.doi.org/10.2138/am-2018-6182

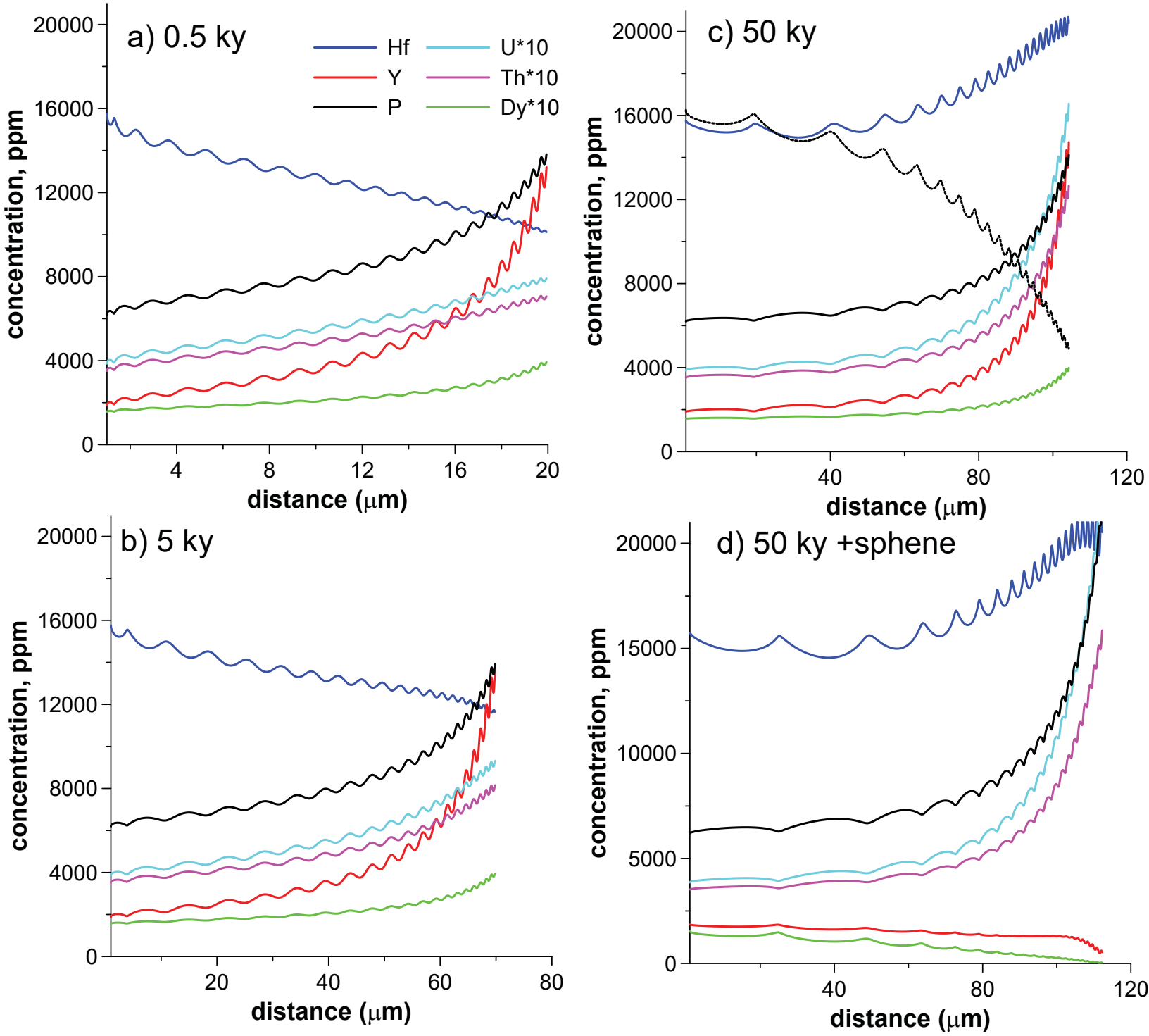

This is a preprint, the final version is subject to change, of the American Mineralogist (MSA)
Cite as Authors (Year) Title. American Mineralogist, in press.
DOI: http://dx.doi.org/10.2138/am-2018-6182

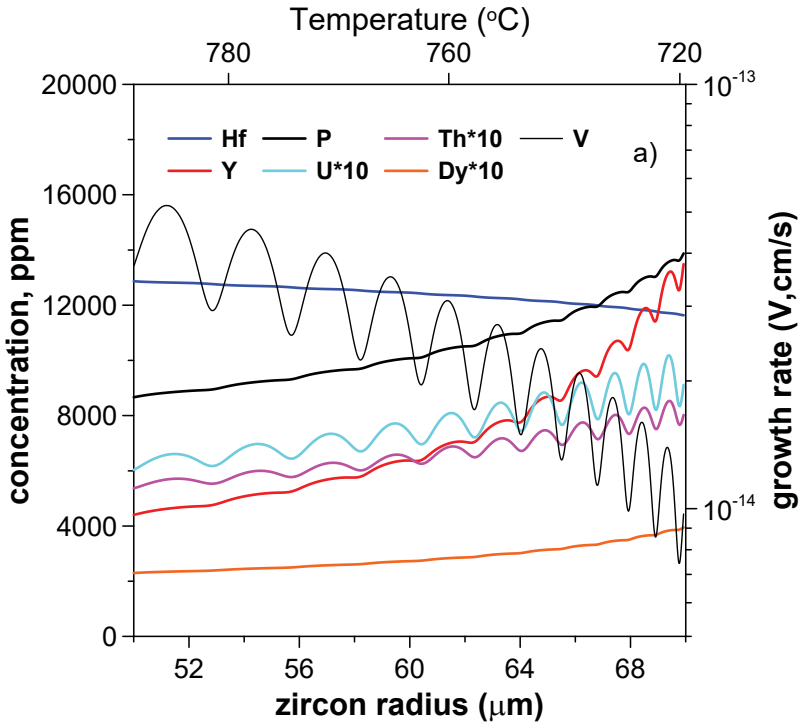

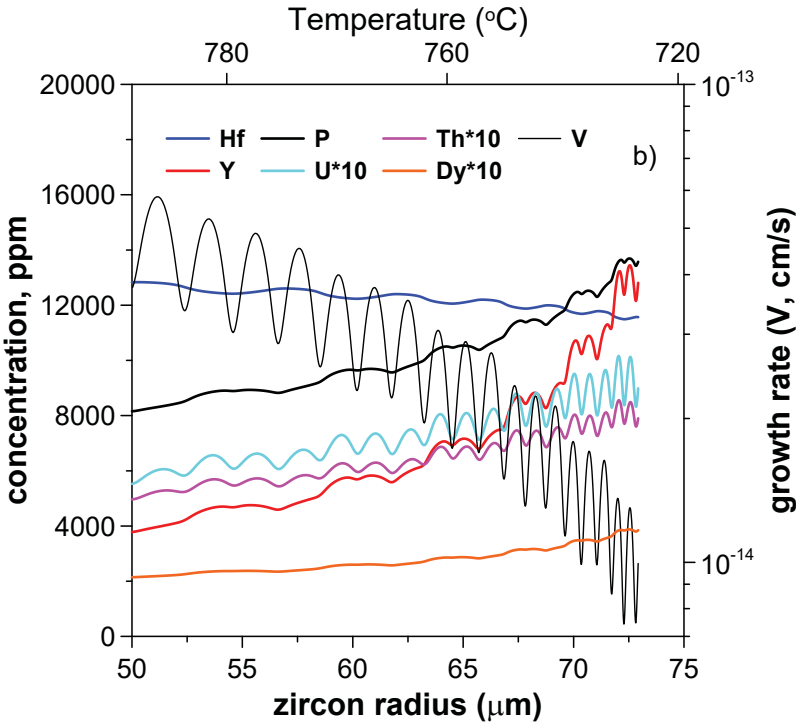

This is a preprint, the final version is subject to change, of the American Mineralogist (MSA)
Cite as Authors (Year) Title. American Mineralogist, in press.
DOI: http://dx.doi.org/10.2138/am-2018-6182